State-space modelling with Steady-State Time Invariant Representation of Energy Based Controllers for Modular Multilevel Converters

Julian Freytes *, Gilbert Bergna †, Jon Are Suul ‡, Salvatore D'Arco ‡, Hani Saad §, Xavier Guillaud *
* Université Lille, Centrale Lille, Arts et Métiers, HEI - EA 2697 - L2EP - Lille, France
† Department of Electric Power Engineering, Norwegian University of Science and Technology - Trondheim, Norway
‡ SINTEF Energy Research - Trondheim, Norway
§ Réseau de Transport d'Électricité (RTE) - La Défense, France

***Abstract*—The average value model of the Modular Multilevel Converter (MMC) is in general non-linear with time periodic variables. Recent developments demonstrated how the MMC model can be transformed into a a Steady-State Time Invariant (SSTI) representation allowing for linearization of the model. While previous modeling efforts for small-signal eigenvalue analysis considered mainly the classical Circulating Current Suppressing Controller (CCSC), this paper presents an approach for representing a complete energy-based control system in a set of Synchronously Rotating Frames (SRFs). This is obtained by separating the state variables according the their frequency components and applying corresponding Park transformations. The resulting model is based on existing controllers implemented in the stationary abc frame, and enables small-signal stability studies of MMCs with such control systems. Simulations results comparing an EMT type MMC model with the complete SSTI system validate the proposed approach.**

***Index Terms*—HVDC Transmission, Modular Multilevel Converter, State-Space Modelling, Energy control, Park transformations.**

I. Introduction

The Modular Multilevel Converter (MMC) has emerged as the most suitable Voltage Source Converter (VSC) topology for HVDC transmission systems [1]. Modelling and controlling the MMC can be considered in general as more challenging compared to two- or three-level VSCs. In particular, MMCs are characterized by additional internal dynamics, related to the internal circulating currents as well as the voltages of the internal distributed capacitors in each arm [2]. Furthermore, multiple frequency components inherently appear in the internal state variables of the MMC [3]. This complicates the procedure of obtaining state-space models with a Steady-State Time-Invariant (SSTI) representation, according to the modelling approaches commonly applied for two-level VSCs [4].

Recently, modeling approaches for obtaining SSTI state-space representation of MMCs in eigenvalue-based small-signal stability analysis of HVDC systems have been proposed in [5], [6]. However, the models in [5] and [6] considered only the case of a classical Circulating Current Suppressing Controller (CCSC) from [7]. With such classical CCSC, it was shown in [8] that the lack of control of the output DC current may cause undesired oscillations and even stability issues. For this reason, more advanced controllers should be considered.

The results in [8] indicate that controllers with explicit control of the internally stored energy of the MMC can be beneficial for avoiding poorly damped dynamics. Such control strategies usually rely on per-phase control loops in the stationary frame, as in [9]. Thus, the control strategies cannot be directly expressed by a SSTI state-space representation. In this paper, a methodology is proposed for transforming MMC control loops implemented in the stationary (abc) frame into a set of rotating (dqz) reference frames. The presented procedure and the resulting representation of the energy-based control system can be combined with the MMC model from [8] to obtain an SSTI representation and a linearized small-signal model of an MMC-based HVDC converter station. The validity of such an SSTI model is confirmed by comparison to the results from a detailed time-domain simulation model of the MMC model with the assumed control system implemented in the stationary frame.

II. Modular Multilevel Converter

A. Arm Averaged Model (AAM) in abc frame

The topology of a three-phase MMC is recalled in Fig. 1. Each phase, $j = a, b, c$ of the converter consists of a leg, having an upper and a lower arm with N submodules (SMs) connected in series. Assuming that all the SMs capacitors voltages in an arm are maintained in a close range, each arm can be represented by an equivalent model, corresponding to the Arm Averaged Model (AAM) shown in Fig. 1 for the lower arm of phase c. Each arm includes an inductance L_{arm}, an equivalent resistance R_{arm} and a capacitor C_{arm} [10].

For deriving the current dynamics of the AAM, the modulation indexes m_j^{Δ} and m_j^{Σ} as well as modulated voltages v_{mj}^{Δ} and v_{mj}^{Σ} are introduced as follows [9]:

$$m_j^{\Delta} \stackrel{\text{def}}{=} m_j^U - m_j^L, \quad m_j^{\Sigma} \stackrel{\text{def}}{=} m_j^U + m_j^L \tag{1}$$

$$v_{mj}^{\Delta} \stackrel{\text{def}}{=} (-v_{mj}^U + v_{mj}^L)/2, \quad v_{mj}^{\Sigma} \stackrel{\text{def}}{=} (v_{mj}^U + v_{mj}^L)/2 \tag{2}$$

The MMC currents can be expressed as in (3).

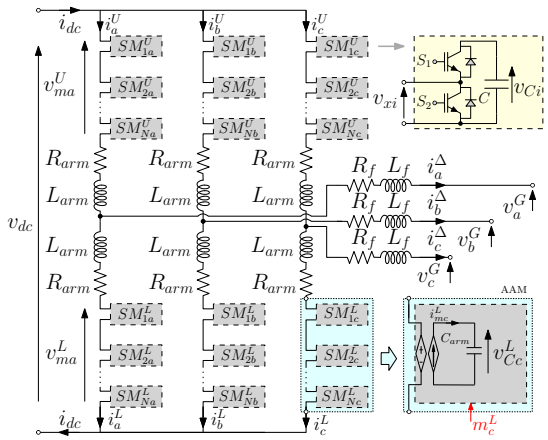

Fig. 1. MMC topology and Arm Averaged Model (AAM).

$$i_j^{\Delta} \stackrel{\text{def}}{=} i_j^U - i_j^L, \quad i_j^{\Sigma} \stackrel{\text{def}}{=} (i_j^U + i_j^L)/2 \tag{3}$$

where i_j^{Δ} corresponds to the AC grid current, and i_j^{Σ} is the common-mode current flowing through the upper and lower arm. The DC-side current i_{dc} is given by the sum of the three currents i_j^{Σ}.

The AC grid current dynamics are expressed as:

$$L_{eq}^{ac} \frac{di_j^{\Delta}}{dt} = v_{mj}^{\Delta} - v_j^G - R_{eq}^{ac} i_j^{\Delta} \tag{4}$$

where $R_{eq}^{ac} \stackrel{\text{def}}{=} (R_{arm} + 2R_f)/2$ and $L_{eq}^{ac} \stackrel{\text{def}}{=} (L_{arm} + 2L_f)/2$. The common-mode arm currents dynamics are given by:

$$L_{arm} \frac{di_j^{\Sigma}}{dt} = \frac{v_{dc}}{2} - v_{mj}^{\Sigma} - R_{arm} i_j^{\Sigma} \tag{5}$$

Finally, the arm capacitors dynamics are given by:

$$2C_{arm} \frac{dv_{Cj}^{\Sigma}}{dt} = m_j^{\Delta} \frac{i_j^{\Delta}}{2} + m_j^{\Sigma} i_j^{\Sigma} \tag{6}$$

$$2C_{arm} \frac{dv_{Cj}^{\Delta}}{dt} = m_j^{\Sigma} \frac{i_j^{\Delta}}{2} + m_j^{\Delta} i_j^{\Sigma} \tag{7}$$

where $v_{Cj}^{\Delta} \stackrel{\text{def}}{=} (v_{Cj}^U - v_{Cj}^L)/2$ and $v_{Cj}^{\Sigma} \stackrel{\text{def}}{=} (v_{Cj}^U + v_{Cj}^L)/2$.

In steady state, the fundamental frequency of the "Δ" variables is the grid frequency ω, while the "Σ" variables contain a component at -2ω and a DC-component [6]. Thus, the variables can be classified as:

- "Δ" *Variables oscillating at* ω: i_j^{Δ}, v_{mj}^{Δ}, m_j^{Δ}, v_{Cj}^{Δ}.
- "Σ" *Variables oscillating at* -2ω: i_j^{Σ}, v_{mj}^{Σ}, m_j^{Σ}, v_{Cj}^{Σ}.

The energy sum W_j^{Σ} is calculated as follows:

$$W_j^{\Sigma} = \frac{1}{2} C_{arm} \left(\left(v_{Cj}^{\Sigma}\right)^2 + \left(v_{Cj}^{\Delta}\right)^2 \right) \tag{8}$$

The energy sum W_j^{Σ} is oscillating mainly at -2ω, and its average value is noted as $\overline{W}_j^{\Sigma}$. The energy difference is calculated as:

$$W_j^{\Delta} = \frac{1}{2} C_{arm} \left(2 v_{Cj}^{\Sigma} v_{Cj}^{\Delta}\right) \tag{9}$$

The energy difference W_j^{Δ} is oscillating mainly at ω, and its average value is noted as $\overline{W}_j^{\Delta}$.

B. Energy-based controller in mixed reference frames

In this section, the assumed MMC control strategy based on the explicit management of the internal energy is presented. For the proper operation of the MMC, the high-level controller must fulfill, in steady state, the specifications illustrated in Fig. 2:

1) Match AC and DC power flows - Fig. 2(a): $P_{ac} \approx P_{dc}$.
2) Horizontal balancing - Fig. 2(b): The average stored energy of each phase-leg $\overline{W}_j^{\Sigma}$ should be controlled.
3) Vertical balancing - Fig. 2(c): The energy difference between the upper and lower arm capacitors $\overline{W}_j^{\Delta}$ should be controlled.

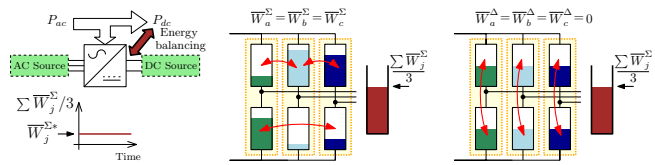

(a) Power match (b) Horizontal balancing (c) Vertical balancing

Fig. 2. Control specifications: graphical description

An overview of the structure for a typical *Energy based* control strategy which verifies the aforementioned specifications is shown in Fig. 3 [9]. In this figure, bold symbols denote vectors. For the AC-side the classical MMC control strategy is based on two cascaded loops. The outer loops controls the active power P_{ac} and reactive power Q_{ac}. The inner loops control the AC currents in dq frame. The currents i_d^{Δ} and i_q^{Δ} are controlled to their references by PI controllers.

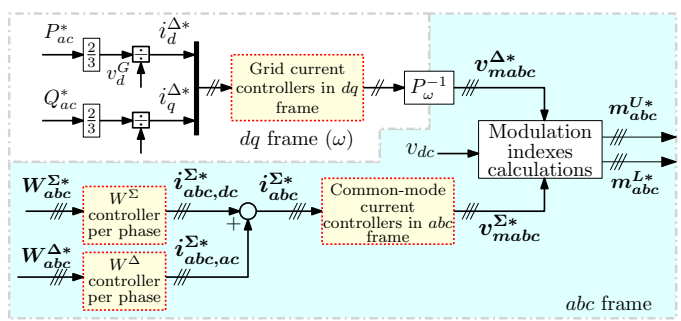

Fig. 3. General scheme *Energy based* control

For controlling the energy sum $\overline{W}_j^{\Sigma}$ for each phase, three independent PI controllers are implemented. The average value $\overline{W}_j^{\Sigma}$ is obtained with a second-order notch filter tuned at 2ω [11]. Setting the same energy reference for each phase (i.e. $\overline{W}_a^{\Sigma *} = \overline{W}_b^{\Sigma *} = \overline{W}_c^{\Sigma *}$), the specification from Fig. 2(b) is assured. These controllers generate the DC component of the common-mode current references $i_{j,dc}^{\Sigma *}$ for the corresponding phase. The detail of the controller structure is shown in Fig. 4.

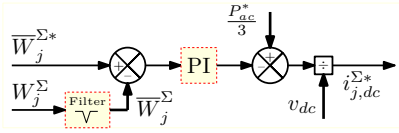

Fig. 4. Energy sum controller (phase j)

The energy difference controller is depicted in Fig. 5, where V^G is the RMS value of the AC grid voltage, $\boldsymbol{R}$ is defined in (10) and $\boldsymbol{K}$ is defined in (11) . This controller guarantees the specification 3 (i.e. vertical balancing). The control details can be found in [12].

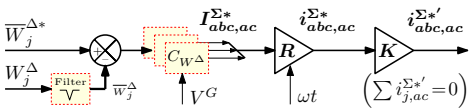

Fig. 5. Energy difference controller

$$\boldsymbol{R} = \sqrt{2}\begin{bmatrix} \cos(\omega t) & 0 & 0 \\ 0 & \cos\left(\omega t - \frac{2\pi}{3}\right) & 0 \\ 0 & 0 & \cos\left(\omega t - \frac{2\pi}{3}\right) \end{bmatrix}. \quad (10)$$

$$\boldsymbol{K} = \begin{bmatrix} 1 & -\frac{1}{2} & -\frac{1}{2} \\ -\frac{1}{2} & 1 & -\frac{1}{2} \\ -\frac{1}{2} & -\frac{1}{2} & 1 \end{bmatrix} \quad (11)$$

The three common-mode currents (for each phase j) are corrected to their references via PI controllers as well [11]. Finally, the modulation signals m_j^U and m_j^L are obtained according to:

$$m_j^U = \frac{-v_{mj}^{\Delta *} - v_{mj}^{\Sigma *}}{v_{dc}} + \frac{1}{2}, \quad m_j^L = \frac{v_{mj}^{\Delta *} - v_{mj}^{\Sigma *}}{v_{dc}} + \frac{1}{2} \quad (12)$$

III. Non-linear time-invariant model using Σ-Δ representation

This section recalls the time-invariant model of the MMC with voltage-based formulation as proposed in [6] and derived from (4), (5), (6) and (7). To achieve a time-invariant model, it is necessary to refer the MMC variables to their corresponding SRFs. For generic variables x^Σ and x^Δ, time-invariant equivalents are obtained with the Park transformation defined in (13) as:

$$\omega \Rightarrow \boldsymbol{x}_{\boldsymbol{dqz}}^{\boldsymbol{\Delta}} \stackrel{\text{def}}{=} \left[x_d^\Delta \; x_q^\Delta \; x_z^\Delta\right]^\top = \boldsymbol{P}_{\boldsymbol{\omega}} \left[x_a^\Delta \; x_b^\Delta \; x_c^\Delta\right]^\top$$
$$-2\omega \Rightarrow \boldsymbol{x}_{\boldsymbol{dqz}}^{\boldsymbol{\Sigma}} \stackrel{\text{def}}{=} \left[x_d^\Sigma \; x_q^\Sigma \; x_z^\Sigma\right]^\top = \boldsymbol{P}_{\boldsymbol{-2\omega}} \left[x_a^\Sigma \; x_b^\Sigma \; x_c^\Sigma\right]^\top$$

$$\boldsymbol{P}_{n\omega} = \frac{2}{3}\begin{bmatrix} \cos(n\omega t) & \cos(n\omega t - \frac{2\pi}{3}) & \cos(n\omega t - \frac{4\pi}{3}) \\ \sin(n\omega t) & \sin(n\omega t - \frac{2\pi}{3}) & \sin(n\omega t - \frac{4\pi}{3}) \\ \frac{1}{2} & \frac{1}{2} & \frac{1}{2} \end{bmatrix} \quad (13)$$

Although the "Σ-Δ" components are classified according to their dominant oscillation frequency, the Σ and Δ quantities are not fully decoupled. This results in time-periodic variables in the equations after applying the above transformations. For the Σ variables, time-periodic terms at 6ω are neglected without compromising the accuracy of the model [6]. Furthermore, the zero sequences of the vectors in "Δ" present time-periodic terms at 3ω. This component was modeled in [6] by means of an auxiliary virtual variable, 90° shifted from the real one, and by using a Park transformation at $+3\omega$ to achieve time invariant signals.

$$3\omega^+ \Rightarrow \boldsymbol{x}_{\boldsymbol{Z}}^{\boldsymbol{\Delta}} \stackrel{\text{def}}{=} \left[x_{Z_d}^\Delta \; x_{Z_q}^\Delta\right]^\top = \boldsymbol{P}_{3\omega} \left[x_z^\Delta \; x_z^{\Delta 90^\circ}\right]^\top$$

Using the above definitions, the MMC dynamics in their "Σ-Δ" representation can be rewritten in a time-invariant form. An overview of the model structure corresponding to the MMC and DC bus equations is shown in Fig. 6 (See [8]).

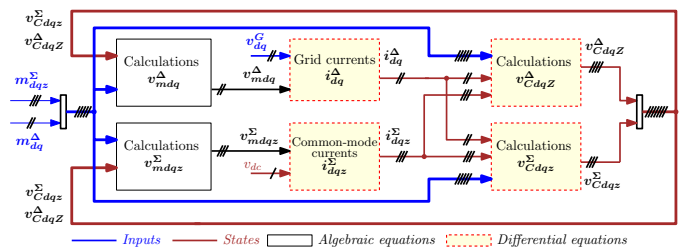

Fig. 6. MMC model with Steady-State Time-Invariant Solution

A. Energy sum calculation in dqz frame

Taking into account (8), the three-phase energy sum $\boldsymbol{W}_{\boldsymbol{abc}}^{\boldsymbol{\Sigma}} = [W_a^\Sigma, \; W_b^\Sigma, \; W_c^\Sigma]^\top$ is calculated as:

$$\boldsymbol{W}_{\boldsymbol{abc}}^{\boldsymbol{\Sigma}} = \frac{1}{2} C_{arm} \boldsymbol{P}_{\boldsymbol{-2\omega}}^{\boldsymbol{-1}} \boldsymbol{v}_{\boldsymbol{Cdqz}}^{\boldsymbol{\Sigma}} \otimes \boldsymbol{P}_{\boldsymbol{-2\omega}}^{\boldsymbol{-1}} \boldsymbol{v}_{\boldsymbol{Cdqz}}^{\boldsymbol{\Sigma}} \cdots \quad (14)$$
$$\cdots + \frac{1}{2} C_{arm} \boldsymbol{P}_{\boldsymbol{\omega}}^{\boldsymbol{-1}} \boldsymbol{v}_{\boldsymbol{Cdqz}}^{\boldsymbol{\Delta}} \otimes \boldsymbol{P}_{\boldsymbol{\omega}}^{\boldsymbol{-1}} \boldsymbol{v}_{\boldsymbol{Cdqz}}^{\boldsymbol{\Delta}}$$

where

$$\boldsymbol{v}_{\boldsymbol{Cdqz}}^{\boldsymbol{\Sigma}} = [v_{Cd}^\Sigma, \; v_{Cq}^\Sigma, \; v_{Cz}^\Sigma]^\top; \quad (15)$$

$$\boldsymbol{v}_{\boldsymbol{Cdqz}}^{\boldsymbol{\Delta}} = \left[v_{Cd}^\Delta, \; v_{Cq}^\Delta, \; v_{Cz}^\Delta\right]^\top \quad (16a)$$
$$v_{Cz}^\Delta = \left(v_{CZ_d}^\Delta \cos(3\omega t) + v_{CZ_q}^\Delta \sin(3\omega t)\right) \quad (16b)$$

It is worth noticing that the operator "$\otimes$" corresponds to an element-wise multiplication of vectors (e.g. $\left[\begin{smallmatrix} a \\ b \end{smallmatrix}\right] \otimes \left[\begin{smallmatrix} c \\ d \end{smallmatrix}\right] = \left[\begin{smallmatrix} ac \\ bd \end{smallmatrix}\right]$). Multiplying (14) by $\boldsymbol{P}_{\boldsymbol{-2\omega}}$ and neglecting the 6th harmonic component (19) is obtained (at the bottom of the following page).

B. Energy difference calculation in dqz frame

Taking into account (9), the three-phase energy difference vector $\boldsymbol{W}_{\boldsymbol{abc}}^{\boldsymbol{\Delta}} = [W_a^\Delta \; W_b^\Delta \; W_c^\Delta]^\top$ is calculated as:

$$\boldsymbol{W}_{\boldsymbol{abc}}^{\boldsymbol{\Delta}} = C_{arm} \left(\boldsymbol{P}_{\boldsymbol{-2\omega}}^{\boldsymbol{-1}} \boldsymbol{v}_{\boldsymbol{Cdqz}}^{\boldsymbol{\Sigma}} \otimes \boldsymbol{P}_{\boldsymbol{\omega}}^{\boldsymbol{-1}} \boldsymbol{v}_{\boldsymbol{Cdqz}}^{\boldsymbol{\Delta}}\right) \quad (20)$$

Multiplying (20) by $\boldsymbol{P_\omega}$, the expression of $\boldsymbol{W^{\Delta}_{dqz}}$ is obtained as in (21).

$$\boldsymbol{W^{\Delta}_{dqz}} = C_{arm}\boldsymbol{P_\omega}\left(\boldsymbol{P^{-1}_{-2\omega}}\boldsymbol{v^{\Sigma}_{Cdqz}} \otimes \boldsymbol{P^{-1}_{\omega}}\boldsymbol{v^{\Delta}_{Cdqz}}\right) \tag{21}$$

The results for the dq components from (21) are time-invariant after neglecting the 6th harmonic component. However, the zero-sequence is pulsating at 3ω, as shown in (22). The same technique as for the zero-sequence component of v^{Δ}_{Cz} may be applied as explained in [6], i.e. creating a virtual system from (22): $W^{\Delta}_{Z_d}$ and $W^{\Delta}_{Z_q}$.

$$\begin{aligned} W^{\Delta}_{z} = C_{arm}\left(v^{\Delta}_{Cd}v^{\Sigma}_{Cd} + v^{\Delta}_{Cq}v^{\Sigma}_{Cq} + 2v^{\Delta}_{CZ_d}v^{\Sigma}_{Cz}\right)\cos(3\omega t) + \ldots \\ \ldots + C_{arm}\left(v^{\Delta}_{Cq}v^{\Sigma}_{Cd} - v^{\Delta}_{Cd}v^{\Sigma}_{Cq} + 2v^{\Delta}_{CZ_q}v^{\Sigma}_{Cz}\right)\sin(3\omega t) \end{aligned} \tag{22}$$

The complete expression of $\boldsymbol{W^{\Delta}_{dqZ}}$ is given in (23) (at the bottom of this page).

IV. SSTI-SRF Representation of Stationary Frame Energy-based controllers

For obtaining the full representation of the system in SRF frame, it is still needed to reformulate the part in stationary frame of the control structure of Fig. 3. This is achieved by referring each part of the controllers to their corresponding SRFs:

- Common-mode current controllers at -2ω.
- Energy sum controllers and averaging filters at -2ω.
- Energy difference controllers and averaging filters at ω.

A. Example of transformation from abc to dqz

In order to illustrate the methodology, the following subsections explains the reformulation of a generic set of three-phase PI controllers in the abc frame, and a second-order notch filter used to extract the average value of the per-phase energy components.

1) Generic PI controller: As an example, let us consider the generic three-phase PI controller in abc frame from Fig. 7. It is controlling the variables $\boldsymbol{X_{abc}} = [X_a \;\; X_b \;\; X_c]^\top$ to their references $\boldsymbol{X^*_{abc}} = [X^*_a \;\; X^*_b \;\; X^*_c]^\top$. The outputs of the controllers are $\boldsymbol{Y_{abc}} = [Y_a \;\; Y_b \;\; Y_c]^\top$, and the states of the integral parts are $\boldsymbol{\xi_{abc}} = [\xi_a \; \xi_b \; \xi_c]^\top$. It is considered that the variables $\boldsymbol{X_{abc}}$ are pulsating at an angular frequency $n\omega$.

The reformulation of the generic PI from Fig. 7 to the SRF frame at $n\omega$ is performed in two steps. First, the integral part of the controller is obtained and second, the controllers output.

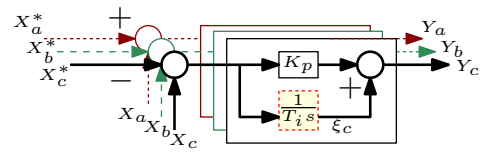

Fig. 7. Generic three-phase PI independent controllers in abc frame

The differential equation of the integral part is:

$$T_i\frac{d\boldsymbol{\xi_{abc}}}{dt} = \boldsymbol{X^*_{abc}} - \boldsymbol{X_{abc}} \tag{24}$$

This equation can be related to the dqz components at $n\omega$ as,

$$T_i\frac{d\boldsymbol{P^{-1}_{n\omega}}\boldsymbol{\xi^{n\omega}_{dqz}}}{dt} = \boldsymbol{P^{-1}_{n\omega}}\boldsymbol{X^{n\omega *}_{dqz}} - \boldsymbol{P^{-1}_{n\omega}}\boldsymbol{X^{n\omega}_{dqz}} \tag{25}$$

where

$$\boldsymbol{\xi^{n\omega}_{dqz}} = \boldsymbol{P_{n\omega}}\boldsymbol{\xi_{abc}}; \boldsymbol{X^{n\omega}_{dqz}} = \boldsymbol{P_{n\omega}}\boldsymbol{X_{abc}}; \boldsymbol{X^{n\omega *}_{dqz}} = \boldsymbol{P_{n\omega}}\boldsymbol{X^*_{abc}} \tag{26}$$

Expanding (25) and multiplying by $\boldsymbol{P_{n\omega}}$ results in (27).

$$T_i\frac{d\boldsymbol{\xi^{n\omega}_{dqz}}}{dt} = \boldsymbol{X^{n\omega *}_{dqz}} - \boldsymbol{X^{n\omega}_{dqz}} - T_i\underbrace{\boldsymbol{P_{n\omega}}\frac{d\boldsymbol{P^{-1}_{n\omega}}}{dt}}_{\boldsymbol{J}_{n\omega}}\boldsymbol{\xi^{n\omega}_{dqz}} \tag{27}$$

where the coupling matrix $\boldsymbol{J_{n\omega}}$ is given by:

$$\boldsymbol{J_{n\omega}} \stackrel{\text{def}}{=} \begin{bmatrix} 0 & n\omega & 0 \\ -n\omega & 0 & 0 \\ 0 & 0 & 0 \end{bmatrix} \tag{28}$$

The output of the controller in abc frame is expressed as,

$$\boldsymbol{Y_{abc}} = \boldsymbol{\xi_{abc}} + K_p\left(\boldsymbol{X^*_{abc}} - \boldsymbol{X_{abc}}\right). \tag{29}$$

With the definitions given in (26), (29) may be written as,

$$\boldsymbol{Y_{abc}} = \boldsymbol{P^{-1}_{n\omega}}\boldsymbol{\xi^{n\omega}_{dqz}} + K_p\left(\boldsymbol{P^{-1}_{n\omega}}\boldsymbol{X^{n\omega *}_{dqz}} - \boldsymbol{P^{-1}_{n\omega}}\boldsymbol{X^{n\omega}_{dqz}}\right) \tag{30}$$

Multiplying (30) by $\boldsymbol{P_{n\omega}}$ yields,

$$\boldsymbol{W^{\Sigma}_{dqz}} = \begin{bmatrix} W^{\Sigma}_d \\ W^{\Sigma}_q \\ W^{\Sigma}_z \end{bmatrix} = \frac{1}{2}C_{arm}\begin{bmatrix} \left(v^{\Delta}_{Cd}\right)^2 - \left(v^{\Delta}_{Cq}\right)^2 + 2v^{\Delta}_{CZ_d}v^{\Delta}_{Cd} + 2v^{\Delta}_{CZ_q}v^{\Delta}_{Cq} + 4v^{\Sigma}_{Cd}v^{\Sigma}_{Cz} \\ 2v^{\Delta}_{Cq}v^{\Delta}_{CZ_d} - 2v^{\Delta}_{Cd}v^{\Delta}_{CZ_q} - 2v^{\Delta}_{Cd}v^{\Delta}_{Cq} + 4v^{\Sigma}_{Cq}v^{\Sigma}_{Cz} \\ \left(v^{\Delta}_{Cd}\right)^2 + \left(v^{\Delta}_{Cq}\right)^2 + \left(v^{\Delta}_{CZ_d}\right)^2 + \left(v^{\Delta}_{CZ_q}\right)^2 + \left(v^{\Sigma}_{Cd}\right)^2 + \left(v^{\Sigma}_{Cq}\right)^2 + 2\left(v^{\Sigma}_{Cz}\right)^2 \end{bmatrix} \tag{19}$$

$$\boldsymbol{W^{\Delta}_{dqZ}} = \begin{bmatrix} W^{\Delta}_d \\ W^{\Delta}_q \\ W^{\Delta}_{Z_d} \\ W^{\Delta}_{Z_q} \end{bmatrix} = C_{arm}\begin{bmatrix} v^{\Delta}_{Cd}v^{\Sigma}_{Cd} + 2v^{\Delta}_{Cd}v^{\Sigma}_{Cz} - v^{\Delta}_{Cq}v^{\Sigma}_{Cq} + v^{\Delta}_{CZ_d}v^{\Sigma}_{Cd} - v^{\Delta}_{CZ_q}v^{\Sigma}_{Cq} \\ 2v^{\Delta}_{Cq}v^{\Sigma}_{Cz} - v^{\Delta}_{Cq}v^{\Sigma}_{Cd} - v^{\Delta}_{Cd}v^{\Sigma}_{Cq} + v^{\Delta}_{CZ_d}v^{\Sigma}_{Cq} + v^{\Delta}_{CZ_q}v^{\Sigma}_{Cd} \\ v^{\Delta}_{Cd}v^{\Sigma}_{Cd} + v^{\Delta}_{Cq}v^{\Sigma}_{Cq} + 2v^{\Delta}_{CZ_d}v^{\Sigma}_{Cz} \\ v^{\Delta}_{Cq}v^{\Sigma}_{Cd} - v^{\Delta}_{Cd}v^{\Sigma}_{Cq} + 2v^{\Delta}_{CZ_q}v^{\Sigma}_{Cz} \end{bmatrix} \tag{23}$$

$$\boldsymbol{Y_{dqz}^{n\omega}} = \boldsymbol{\xi_{dqz}^{n\omega}} + K_p\left(\boldsymbol{X_{dqz}^{n\omega *}} - \boldsymbol{X_{dqz}^{n\omega}}\right) \tag{31}$$

The complete PI structure in dqz frame at $n\omega$ is determined by (27) and (31). These results are expressed in block-diagram form in Fig. 8.

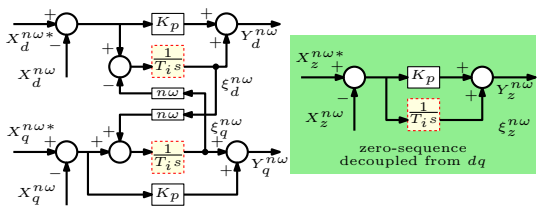

Fig. 8. Generic three-phase PI controllers from Fig. 7 in dqz frame

The model from Fig. 8 is the result of applying the Park transformation to the three-phase PI controllers from Fig. 7. It can be noted that the cross-couplings in the model represents the phase-shift resulting from the application of PI controllers for tracking sinusoidal signals, and should not be confused with decoupling terms in a dq current controller.

2) Second order notch filter: The filters used for the energies $\boldsymbol{W_{abc}^{\Sigma}}$ and $\boldsymbol{W_{abc}^{\Delta}}$ are second order notch filters tuned at their corresponding frequencies. As an example, let us consider the three phase signals $\boldsymbol{U_{abc}} = [U_a U_b U_c]^\top$ and the filtered values $\overline{\boldsymbol{Y}}_{\boldsymbol{abc}} = [\overline{Y}_a \overline{Y}_b \overline{Y}_c]^\top$. The second order transfer function of the notch filter for the phase j is:

$$\frac{\overline{Y}_j}{U_j} = \frac{s^2 + \omega_n^2}{s^2 + 2\zeta\omega_n s + \omega_n^2} \tag{32}$$

where ω_n is the natural frequency and ζ is the damping coefficient. Equation (32) may be written as a second order differential function as:

$$\frac{d^2\overline{Y}_j}{dt^2} + 2\zeta\omega_n\frac{d\overline{Y}_j}{dt} + \omega_n^2\overline{Y}_j = \frac{d^2U_j}{dt^2} + \omega_n^2 U_j \tag{33}$$

Choosing the following state variables:

$$F_{1j} \stackrel{\text{def}}{=} \overline{Y}_j - U_j \tag{34a}$$

$$F_{2j} \stackrel{\text{def}}{=} \frac{d\overline{Y}_j}{dt} - \frac{dU_j}{dt} + 2\zeta\omega_n F_{1j} + 2\zeta\omega_n U_j \tag{34b}$$

The output of the notch filter can be obtained directly from (34a). Derivating the states from (34) and generalizing for a three-phase system it is obtained:

$$\frac{d\boldsymbol{F_{1abc}}}{dt} = \boldsymbol{F_{2abc}} - 2\zeta\omega_n\boldsymbol{F_{1abc}} - 2\zeta\omega_n\boldsymbol{U_{abc}} \tag{35a}$$

$$\frac{d\boldsymbol{F_{2abc}}}{dt} = -\omega_n^2\boldsymbol{F_{1abc}} \tag{35b}$$

$$\overline{\boldsymbol{Y}}_{\boldsymbol{abc}} = \boldsymbol{F_{1abc}} + \boldsymbol{U_{abc}} \tag{35c}$$

where $\boldsymbol{F_{1abc}} = [F_{1a}F_{1b}F_{1c}]^\top$ and $\boldsymbol{F_{2abc}} = [F_{2a}F_{2b}F_{2c}]^\top$.

Equation (35) can be transformed into the SRF as:

$$\frac{d\boldsymbol{F_{1dqz}}}{dt} = \boldsymbol{F_{2dqz}} - 2\zeta\omega_n\boldsymbol{F_{1dqz}} - 2\zeta\omega_n\boldsymbol{U_{dqz}} - \boldsymbol{J_{n\omega}}\boldsymbol{F_{1dqz}} \tag{36a}$$

$$\frac{d\boldsymbol{F_{2dqz}}}{dt} = -\omega_n^2\boldsymbol{F_{1dqz}} - \boldsymbol{J_{n\omega}}\boldsymbol{F_{2dqz}} \tag{36b}$$

$$\overline{\boldsymbol{Y}}_{\boldsymbol{dqz}} = \boldsymbol{F_{1dqz}} + \boldsymbol{U_{dqz}} \tag{36c}$$

where $\boldsymbol{F_{1dqz}} = [F_{1d}F_{1q}F_{1z}]^\top$, $\boldsymbol{F_{2dqz}} = [F_{2d}F_{2q}F_{2z}]^\top$, $\boldsymbol{U_{dqz}} = [U_d U_q U_z]^\top$ and $\overline{\boldsymbol{Y}}_{\boldsymbol{dqz}} = [\overline{Y}_d \overline{Y}_q \overline{Y}_z]^\top$. Equation (36) summarizes the three-phase notch filter in dqz frame.

B. Energy sum controller reformulation

The PI controller and the notch filter expressed in dqz frame are obtained with the methodology explained in section IV-A with $n = -2$ applied to the controller and the filter from Fig. 4.

1) Averaging filter: The energy sum $\boldsymbol{W_{abc}^{\Sigma}}$ is filtered to obtain $\overline{\boldsymbol{W}}_{\boldsymbol{abc}}^{\boldsymbol{\Sigma}}$ before sending the signals to the PI controller in abc frame (Fig. 4) with a notch filter. Considering (36) and:

$$\boldsymbol{W_{abc}^{\Sigma}} = \boldsymbol{P_{-2\omega}^{-1}}\boldsymbol{W_{dqz}^{\Sigma}}; \quad \overline{\boldsymbol{W}}_{\boldsymbol{abc}}^{\boldsymbol{\Sigma}} = \boldsymbol{P_{-2\omega}^{-1}}\overline{\boldsymbol{W}}_{\boldsymbol{dqz}}^{\boldsymbol{\Sigma}} \tag{37}$$

the notch filter of $\boldsymbol{W_{dqz}^{\Sigma}}$ is expressed as in (38) with $\omega_n = 2\omega$.

$$\frac{d\boldsymbol{F_{1dqz}^{\Sigma}}}{dt} = \boldsymbol{F_{2dqz}^{\Sigma}} - 4\zeta\omega\boldsymbol{F_{1dqz}^{\Sigma}} - 4\zeta\omega\boldsymbol{W_{dqz}^{\Sigma}} - \boldsymbol{J_{-2\omega}}\boldsymbol{F_{1dqz}^{\Sigma}} \tag{38a}$$

$$\frac{d\boldsymbol{F_{2dqz}^{\Sigma}}}{dt} = -4\omega^2\boldsymbol{F_{1dqz}^{\Sigma}} - \boldsymbol{J_{-2\omega}}\boldsymbol{F_{2dqz}^{\Sigma}} \tag{38b}$$

$$\overline{\boldsymbol{W}}_{\boldsymbol{dqz}}^{\boldsymbol{\Sigma}} = \boldsymbol{F_{1dqz}^{\Sigma}} + \boldsymbol{W_{dqz}^{\Sigma}} \tag{38c}$$

2) PI controller: The PI controller expressed in dqz frame is obtained with the methodology explained in IV-A1 with $n\omega = -2\omega$ applied to the controller from Fig. 4. The result is shown in (39). The controller output is expressed in (40).

$$T_i^{W^\Sigma}\frac{d\boldsymbol{\xi_{dqz}^{W^\Sigma}}}{dt} = \overline{\boldsymbol{W}}_{\boldsymbol{dqz}}^{\boldsymbol{\Sigma *}} - \overline{\boldsymbol{W}}_{\boldsymbol{dqz}}^{\boldsymbol{\Sigma}} - T_i^{W^\Sigma}\boldsymbol{J_{-2\omega}}\boldsymbol{\xi_{dqz}^{W^\Sigma}} \tag{39}$$

$$\boldsymbol{i_{dqz,dc}^{\Sigma *}} = \begin{bmatrix} 0 \\ 0 \\ \frac{P_{ac}^*}{3v_{dc}} \end{bmatrix} - \frac{\left(\boldsymbol{\xi_{dqz}^{W^\Sigma}} + K_p^{W^\Sigma}\left(\overline{\boldsymbol{W}}_{\boldsymbol{dqz}}^{\boldsymbol{\Sigma *}} - \overline{\boldsymbol{W}}_{\boldsymbol{dqz}}^{\boldsymbol{\Sigma}}\right)\right)}{v_{dc}} \tag{40}$$

The reference values for $\overline{\boldsymbol{W}}_{\boldsymbol{dq}}^{\boldsymbol{\Sigma *}}$ are set to zero while the zero-sequence component $\overline{W}_z^{\Sigma *}$ is set proportional to the desired total energy stored in the MMC.

C. Energy-difference controller reformulation

1) Averaging filter: The energy sum $\boldsymbol{W_{abc}^{\Delta}}$ is filtered to obtain $\overline{\boldsymbol{W}}_{\boldsymbol{abc}}^{\boldsymbol{\Delta}}$ before sending the signals to the PI controller in abc frame with a notch filter (Fig. 5). Considering the vectors $\boldsymbol{W_{abc}^{\Delta}}$ and $\overline{\boldsymbol{W}}_{\boldsymbol{abc}}^{\boldsymbol{\Delta}}$, where the zero-sequence components are expressed as a function of their respectives Z_d and Z_q components: $\boldsymbol{W_{abc}^{\Delta}} = \boldsymbol{P_{\omega}^{-1}}\left[W_d^\Delta\ W_q^\Delta\ W_{Z_d}^\Delta\cos(3\omega t) + W_{Z_q}^\Delta\sin(3\omega t)\right]^\top$ and

$$\overline{\boldsymbol{W}}^{\boldsymbol{\Delta}}_{\boldsymbol{abc}} = \boldsymbol{P}^{\boldsymbol{-1}}_{\boldsymbol{\omega}} \left[\overline{W}^{\Delta}_{d}\ \overline{W}^{\Delta}_{q}\ \overline{W}^{\Delta}_{Z_d}\cos(3\omega t) + \overline{W}^{\Delta}_{Z_q}\sin(3\omega t)\right]^{\top};$$

the notch filter of $\boldsymbol{W}^{\boldsymbol{\Delta}}_{\boldsymbol{dqZ}}$ in dqZ frame is expressed as:

$$\frac{d\boldsymbol{F}^{\boldsymbol{\Delta}}_{\boldsymbol{1dqZ}}}{dt} = \boldsymbol{F}^{\boldsymbol{\Delta}}_{\boldsymbol{2dqZ}} - \boldsymbol{J_G}\boldsymbol{F}^{\boldsymbol{\Delta}}_{\boldsymbol{1dqZ}} - 2\zeta\omega\left(\boldsymbol{W}^{\boldsymbol{\Delta}}_{\boldsymbol{dqZ}} + \boldsymbol{F}^{\boldsymbol{\Delta}}_{\boldsymbol{1dqZ}}\right) \quad (41a)$$

$$\frac{d\boldsymbol{F}^{\boldsymbol{\Delta}}_{\boldsymbol{2dqZ}}}{dt} = -\omega^2\boldsymbol{F}^{\boldsymbol{\Delta}}_{\boldsymbol{1dqZ}} - \boldsymbol{J_G}\boldsymbol{F}^{\boldsymbol{\Delta}}_{\boldsymbol{2dqZ}} \quad (41b)$$

$$\overline{\boldsymbol{W}}^{\boldsymbol{\Delta}}_{\boldsymbol{dqZ}} = \boldsymbol{W}^{\boldsymbol{\Delta}}_{\boldsymbol{dqZ}} + \boldsymbol{F}^{\boldsymbol{\Delta}}_{\boldsymbol{1dqZ}} \quad (41c)$$

where,

$$\boldsymbol{J_G} \stackrel{\text{def}}{=} \begin{bmatrix} \boldsymbol{C_\omega} & \boldsymbol{0_{2\times 2}} \\ \boldsymbol{0_{2\times 2}} & 3\boldsymbol{C_\omega} \end{bmatrix}; \quad \boldsymbol{C_\omega} \stackrel{\text{def}}{=} \begin{bmatrix} 0 & \omega \\ -\omega & 0 \end{bmatrix} \quad (42)$$

2) PI controller: The PI controller from Fig. 5 is referred to the dqZ axes. The same procedure as before is used on the zero-sequence component, where the state of the integral part is now:

$$\boldsymbol{\xi}^{\boldsymbol{W^\Delta}}_{\boldsymbol{dqZ}} = \left[\xi^{W^\Delta}_{d}\ \xi^{W^\Delta}_{q}\ \xi^{W^\Delta}_{Z_d}\ \xi^{W^\Delta}_{Z_q}\right]^{\top} \quad (43)$$

The result of the integral part is given in (44).

$$T^{W^\Delta}_{i}\frac{d\boldsymbol{\xi}^{\boldsymbol{W^\Delta}}_{\boldsymbol{dqZ}}}{dt} = \overline{\boldsymbol{W}}^{\boldsymbol{\Delta *}}_{\boldsymbol{dqZ}} - \overline{\boldsymbol{W}}^{\boldsymbol{\Delta}}_{\boldsymbol{dqZ}} - T^{W^\Delta}_{i}\boldsymbol{J_G}\boldsymbol{\xi}^{\boldsymbol{W^\Delta}}_{\boldsymbol{dqZ}} \quad (44)$$

The output of the PI controller is obtained applying the Park transformation at ω and 3ω to the control law from Fig. 5, which yields:

$$\boldsymbol{I}^{\boldsymbol{\Sigma *}}_{\boldsymbol{dqZ,ac}} = -\tfrac{1}{V^G}\left(\boldsymbol{\xi}^{\boldsymbol{W\Delta}}_{\boldsymbol{dqZ}} + K^{W\Delta}_{p}\left(\overline{\boldsymbol{W}}^{\boldsymbol{\Delta *}}_{\boldsymbol{dqZ}} - \overline{\boldsymbol{W}}^{\boldsymbol{\Delta}}_{\boldsymbol{dqZ}}\right)\right) \quad (45)$$

For multiplying the output of the energy-difference controller by the matrix $\boldsymbol{R}$ and $\boldsymbol{K}$ defined in (10) and (11) respectively, it is necessary to obtain the three-phase vector $\boldsymbol{I}^{\boldsymbol{\Sigma *}}_{\boldsymbol{abc,ac}}$ as a function of the components dqZ, which is obtained as:

$$\boldsymbol{I}^{\boldsymbol{\Sigma *}}_{\boldsymbol{abc,ac}} = \boldsymbol{P}^{\boldsymbol{-1}}_{\boldsymbol{\omega}}\begin{bmatrix} I^{\Sigma *}_{d,ac} \\ I^{\Sigma *}_{q,ac} \\ I^{\Sigma *}_{Zd,ac}\cos(3\omega t) + I^{\Sigma *}_{Zq,ac}\sin(3\omega t) \end{bmatrix} \quad (46)$$

Note that the inverse Park transformation in Fig. (46) has a frequency of ω and not 2ω as the other "Σ" variables. The reason is that the frequency of the "ac" component of the current i^{Σ} reference used for balancing the W^{Δ} is ω.

Finally, for obtaining the common-mode currents reference in dqz frame, the Park transformation at 2ω is applied to the controllers output from Fig. 5. The results are shown in (47) where the 6th harmonic has been neglected.

$$\boldsymbol{P}_{\boldsymbol{-2\omega}}\boldsymbol{i}^{\boldsymbol{\Sigma *'}}_{\boldsymbol{abc,ac}} = \boldsymbol{P}_{\boldsymbol{-2\omega}}\left(\boldsymbol{KRI}^{\boldsymbol{\Sigma *}}_{\boldsymbol{abc,ac}}\right) \quad (47a)$$

$$\boldsymbol{i}^{\boldsymbol{\Sigma *'}}_{\boldsymbol{dqz,ac}} = \frac{3}{2\sqrt{2}}\begin{bmatrix} I^{\Sigma *}_{d,ac} + I^{\Sigma *}_{Zd,ac} \\ I^{\Sigma *}_{q,ac} + I^{\Sigma *}_{Zq,ac} \\ 0 \end{bmatrix} \quad (47b)$$

D. Complete control structure

The complete control structure represented in dqz coordinates shown in Fig. 9. The grid current controller for $\boldsymbol{i}^{\boldsymbol{\Delta}}_{\boldsymbol{dq}}$ and modulation indexes calculations $\boldsymbol{m}^{\boldsymbol{\Delta}}_{\boldsymbol{dq}}$ and $\boldsymbol{m}^{\boldsymbol{\Sigma}}_{\boldsymbol{dqz}}$ is performed in the same way as in [8]. The common-mode current controllers for $\boldsymbol{i}^{\boldsymbol{\Sigma}}_{\boldsymbol{dqz}}$ is obtained from Fig. 8 with $n = -2\omega$. The current and energy control loops are tuned for a response time of 5ms and 50ms respectively.

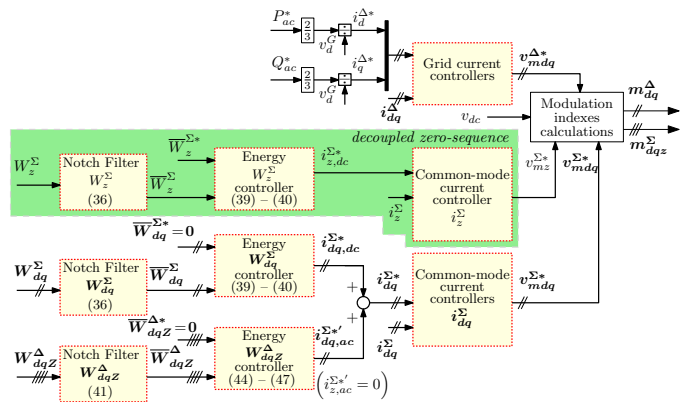

Fig. 9. Complete structure *Energy based* control in SRFs — Mathematical equivalence of Fig. 3.

This controller resulted from the transcription of the scheme from Fig. 3 to dqz frame. It is important to note that this formulation highlights the decoupling of the z-sequence of the energy sum W^{Σ}_{z} (proportional to the total stored energy) and the common-mode current i^{Σ}_{z} (proportional to the DC current).

V. Simulation results

To validate the developed complete SSTI model of the MMC with *Energy based* control, results from simulation of a single converter with two different models will be shown and discussed in the following:

1) *EMT*: The system from Fig. 1 implemented in EMTP-RV with 400 SMs. The MMC is modeled with the so-called "Model #2: *Equivalent Circuit-Based Model*" from [10]. The controller is implemented in abc frame (Fig. 3, [9]).
2) *SSTI*: Non-Linear Time-Invariant state-space model, with the MMC dynamics represented according to Fig. 6 and the control system represented according to Fig. 9.

Starting with an AC power transfer of 1pu, a step on Q^{*}_{ac} of 0.1pu is applied at $t = 20$ms. At $t = 120$ms, a step on P^{*}_{ac} of -0.3pu is applied. Simulation results for the grid and common-mode currents are gathered in Fig. 10 and the energy sum and difference in Fig. 11. The error ε is calculated for each variable y as $\varepsilon(t) = |y_{EMT}(t) - y_{SSTI}(t)|$, where $y_{EMT}(t)$ is the time domain result of the EMTP-RV simulation and $y_{SSTI}(t)$ is the result of the SSTI model.

The error computed for the grid currents $\boldsymbol{i}^{\boldsymbol{\Delta}}_{\boldsymbol{dq}}$ in Fig. 10(a) is less than 0.3%, and the common mode currents $\boldsymbol{i}^{\boldsymbol{\Sigma}}_{\boldsymbol{dq}}$ in Fig. 10(b) the error is less than 1% in steady state and 2% during transients. The currents $\boldsymbol{i}^{\boldsymbol{\Sigma}}_{\boldsymbol{dq}}$ presents a steady-state value different than zero, which results in a circulating current in

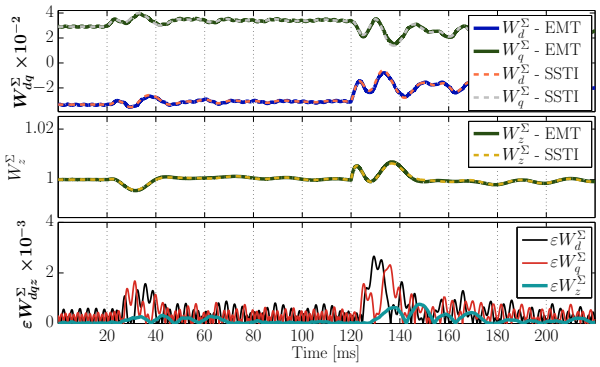

(a) Energy sum $\boldsymbol{W}_{dqz}^{\Sigma}$ pu

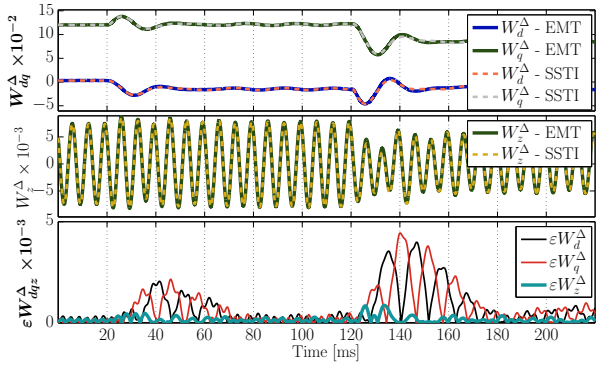

(b) Energy difference $\boldsymbol{W}_{dqz}^{\Delta}$ pu

Fig. 11. Time domain validation – Energy – EMT: EMTP-RV simulation, $SSTI$: Non-linear time-invariant model in Simulink

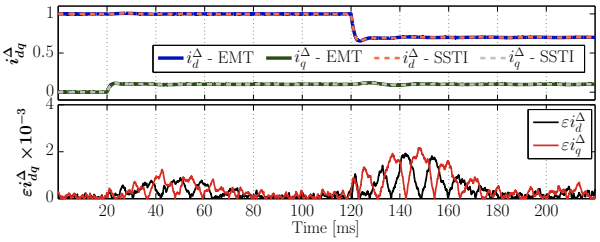

(a) Grid currents $\boldsymbol{i}_{dq}^{\Delta}$ pu

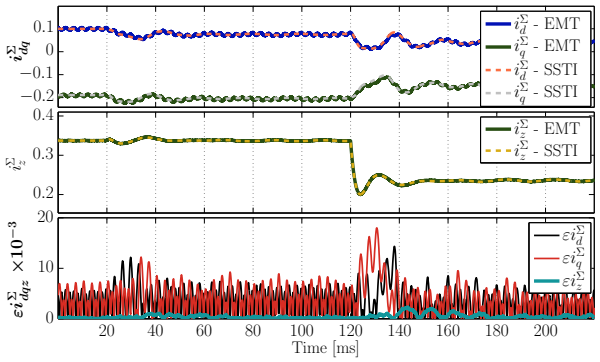

(b) Common-mode currents $\boldsymbol{i}_{dqz}^{\Sigma}$ pu

Fig. 10. Time domain validation – Currents – EMT: EMTP-RV simulation, $SSTI$: Non-linear time-invariant model in Simulink

steady state inside the converter. There are two main reasons: the use of Uncompensated-Modulation (UCM) [6] and the natural coupling of the PI controllers in abc frame (Fig. 8). Nevertheless, the same behavior is observed in both models, validating the results. Finally, the error for i_z^Σ is less than 0.2%.

Results from Figs. 10 and 11 proves the validity of the proposed approach.

VI. Conclusions

This paper presented a modelling approach for obtaining SSTI representation in a synchronous rotating frame of an existing energy-based MMC control system implemented in the stationary abc frame. This representation highlights the decoupling of the total stored energy control (zero-sequence of the energy-sum) and the direct-quadrature energies. The resulting system was compared against a 401-level MMC implemented in EMTP-RV, validating the obtained SSTI representation of the MMC and the energy based controller. The derived formulation of the energy controller may be a starting point for developing improved energy-based control structures for the MMC.

References

[1] A. Lesnicar and R. Marquardt, "An innovative modular multilevel converter topology suitable for a wide power range," in *Power Tech Conference Proceedings, 2003 IEEE Bologna*, vol. 3, pp. 6 pp. Vol.3–, June 2003.

[2] A. Antonopoulos, L. Angquist, and H. P. Nee, "On dynamics and voltage control of the modular multilevel converter," in *Power Electronics and Applications, 2009. EPE '09. 13th European Conference on*, pp. 1–10, Sept 2009.

[3] L. Harnefors, A. Antonopoulos, S. Norrga, L. Angquist, and H.-P. Nee, "Dynamic analysis of modular multilevel converters," *Industrial Electronics, IEEE Transactions on*, vol. 60, pp. 2526–2537, July 2013.

[4] P. Rault, F. Colas, X. Guillaud, and S. Nguefeu, "Method for small signal stability analysis of vsc-mtdc grids," in *Power and Energy Society General Meeting, 2012 IEEE*, pp. 1–7, July 2012.

[5] A. Jamshidifar and D. Jovcic, "Small-signal dynamic dq model of modular multilevel converter for system studies," *IEEE Transactions on Power Delivery*, vol. 31, pp. 191–199, Feb 2016.

[6] G. Bergna, J. A. Suul, and S. D'Arco, "State-space modelling of modular multilevel converters for constant variables in steady-state," in *2016 IEEE 17th Workshop on Control and Modeling for Power Electronics (COMPEL)*, pp. 1–9, June 2016.

[7] Q. Tu, Z. Xu, and J. Zhang, "Circulating current suppressing controller in modular multilevel converter," in *IECON 2010 - 36th Annual Conference on IEEE Industrial Electronics Society*, pp. 3198–3202, Nov 2010.

[8] J. Freytes, G. Bergna, J. A. Suul, S. D'Arco, H. Saad, and X. Guillaud, "Small-signal model analysis of droop-controlled modular multilevel converters with circulating current suppressing controller," in *13th IET International Conference on AC and DC Power Transmission, 2017*, 14-16 February 2017.

[9] H. Saad, X. Guillaud, J. Mahseredjian, S. Dennetire, and S. Nguefeu, "Mmc capacitor voltage decoupling and balancing controls," *IEEE Transactions on Power Delivery*, vol. 30, pp. 704–712, April 2015.

[10] H. Saad, S. Dennetiere, J. Mahseredjian, P. Delarue, X. Guillaud, J. Peralta, and S. Nguefeu, "Modular multilevel converter models for electromagnetic transients," *Power Delivery, IEEE Transactions on*, vol. 29, pp. 1481–1489, June 2014.

[11] A. Ferreira, C. Collados, O. Gomis-Bellmunt, and M. Teixido, "Modular multilevel converter electrical circuit model for hvdc applications," in *Power Electronics and Applications (EPE'15 ECCE-Europe), 2015 17th European Conference on*, pp. 1–10, Sept 2015.

[12] K. Shinoda, J. Freytes, A. Benchaib, J. Dai, H. Saad, and X. Guillaud, "Energy difference controllers for MMC without DC current perturbations," in *2nd International Conference on HVDC (HVDC2016 - CIGRE)*, Oct 2016.